AGU ADVANCING EARTH AND SPACE SCIENCES

Earth and Space Science

RESEARCH ARTICLE
10.1029/2023EA003322

Special Section:
The Perseverance Rover's Exploration of the Western Fan Front, Jezero Crater, Mars

Oriented Bedrock Samples Drilled by the Perseverance Rover on Mars

Benjamin P. Weiss[1], Elias N. Mansbach[1], Joseph L. Carsten[2], Kyle W. Kaplan[2], Justin N. Maki[2], Roger C. Wiens[3], Tanja Bosak[1], Curtis L. Collins[2], Jennifer Fentress[1], Joshua M. Feinberg[4], Yulia Goreva[2], Megan Kennedy Wu[5], Tara A. Estlin[2], Douglas E. Klein[2], Rachel E. Kronyak[2], Robert C. Moeller[2], Nicholas Peper[2], Adriana Reyes-Newell[6], Mark A. Sephton[7], David L. Shuster[8], Justin I. Simon[9], Kenneth H. Williford[10], Kathryn W. Stack[2], and Kenneth A. Farley[11]

[1]Department of Earth, Atmospheric and Planetary Sciences, Massachusetts Institute of Technology, Cambridge, MA, USA, [2]Jet Propulsion Laboratory, California Institute of Technology, Pasadena, CA, USA, [3]Department of Earth, Atmospheric, and Planetary Sciences, Purdue University, West Lafayette, IN, USA, [4]Department of Earth and Environmental Sciences, Institute for Rock Magnetism, University of Minnesota, Minneapolis, MN, USA, [5]Malin Space Science Systems, Inc., San Diego, CA, USA, [6]Southwest Sciences, Inc., Santa Fe, NM, USA, [7]Department of Earth Sciences and Engineering, Imperial College London, London, UK, [8]Department of Earth and Planetary Science, University of California, Berkeley, Berkeley, CA, USA, [9]Astromaterials Research and Exploration Science Division, Center for Isotope Cosmochemistry and Geochronology, NASA Johnson Space Center, Houston, TX, USA, [10]Blue Marble Space Institute of Science, Seattle, WA, USA, [11]Division of Geological and Planetary Sciences, California Institute of Technology, Pasadena, CA, USA

Benjamin P. Weiss and Elias N. Mansbach contributed equally to this work.

Key Points:

- The Perseverance rover has acquired drill cores of Martian igneous and sedimentary bedrock for future potential return to Earth
- Using rover engineering data, we have oriented all rock cores in Martian geographic coordinates to better than 2.7° uncertainty
- Orientation enables future studies of the paleodirections associated with Martian magmatic, sedimentary, tectonic, and magnetic processes

Supporting Information:

Supporting Information may be found in the online version of this article.

Correspondence to:

B. P. Weiss,
bpweiss@mit.edu

Citation:

Weiss, B. P., Mansbach, E. N., Carsten, J. L., Kaplan, K. W., Maki, J. N., Wiens, R. C., et al. (2024). Oriented bedrock samples drilled by the Perseverance rover on Mars. *Earth and Space Science*, *11*, e2023EA003322. https://doi.org/10.1029/2023EA003322

Received 27 SEP 2023
Accepted 18 DEC 2023

Author Contributions:

Conceptualization: Benjamin P. Weiss, Justin I. Simon, Kenneth H. Williford
Formal analysis: Benjamin P. Weiss, Elias N. Mansbach, Kyle W. Kaplan, Nicholas Peper
Funding acquisition: Benjamin P. Weiss, Roger C. Wiens

Abstract A key objective of the Perseverance rover mission is to acquire samples of Martian rocks for future return to Earth. Eventual laboratory analyses of these samples would address key questions about the evolution of the Martian climate, interior, and habitability. Many such investigations would benefit greatly from samples of Martian bedrock that are oriented in absolute Martian geographic coordinates. However, the Mars 2020 mission was designed without a requirement for orienting the samples. Here we describe a methodology that we developed for orienting rover drill cores in the Martian geographic frame and its application to Perseverance's first 20 rock samples. To orient the cores, three angles were measured: the azimuth and hade of the core pointing vector (i.e., vector oriented along the core axis) and the core roll (i.e., the solid body angle of rotation around the pointing vector). We estimated the core pointing vector from the attitude of the rover's Coring Drill during drilling. To orient the core roll, we used oriented images of asymmetric markings on the bedrock surface acquired with the rover's Wide Angle Topographic Sensor for Operations and eNgineering (WATSON) camera. For most samples, these markings were in the form of natural features on the outcrop, while for four samples they were artificial ablation pits produced by the rover's SuperCam laser. These cores are the first geographically-oriented (<2.7° 3σ total uncertainty) bedrock samples from another planetary body. This will enable a diversity of paleomagnetic, sedimentological, igneous, tectonic, and astrobiological studies on the returned samples.

Plain Language Summary The central goal of the Perseverance rover is to drill rock samples that can be brought back to Earth. Future laboratory studies of these samples could tell us about the history of Mars' climate, its interior structure and whether it was once habitable. These studies would greatly benefit from information about how the rock samples were oriented relative to Martian geographic coordinates. Here we show how we developed a technique to orient cores drilled by the rover and applied it to Perseverance's first 20 rock samples. Like all methods for orienting three-dimensional objects, this required measuring three angles which are analogous to the pitch, yaw, and roll of a boat. We measured the the first two angles using the known orientation of the rover arm during drilling. We measured the third angle using rover photographs of markings on the rock face prior to drilling. These markings were either natural features on the outcrop or, for rock faces with no clear natural markings, an artificial L-shaped pattern of pits produced by the rover's laser. These cores are the first geographically-oriented samples of bedrock from another planet. This will enable a diversity of geological, geophysical, and paleontological studies on the samples in Earth laboratories.

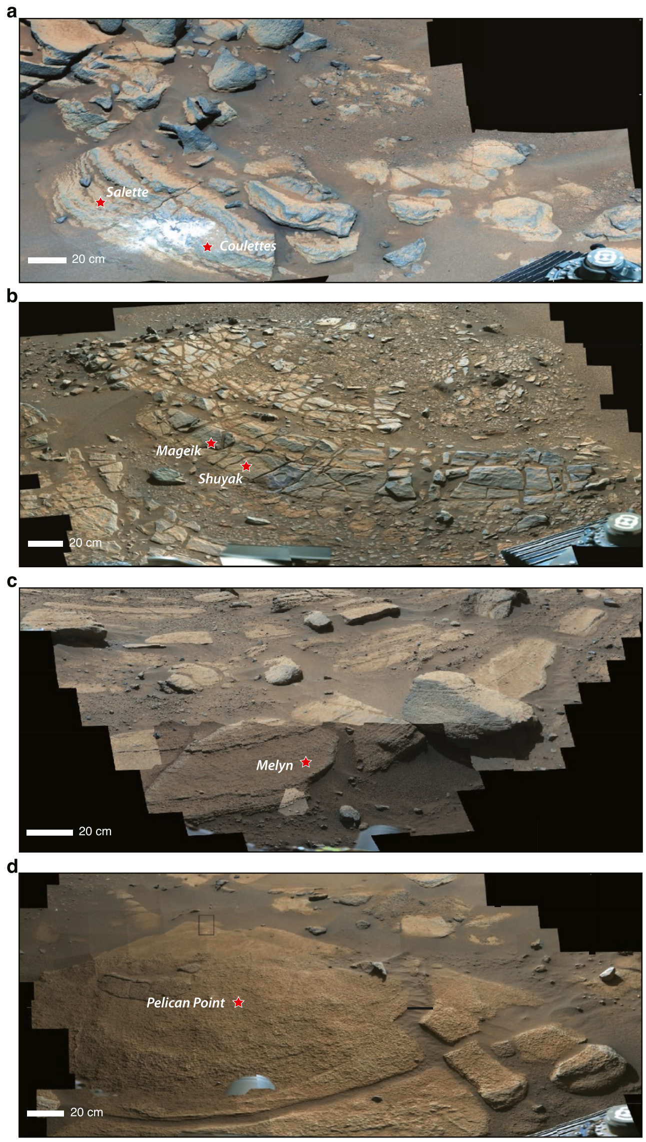
a
Salette
Coulettes
20 cm
b
Mageik
Shuyak
20 cm
c
Melyn
20 cm
d
Pelican Point
20 cm

Table 1
Orientations of the First 23 Coring Attempts by the Perseverance Rover

Sample	Workspace	Sol	Lithology	Bedrock?	Hade (°)	Azimuth (°)	Roll (°)
Roubion[a]	Roubion	164	Igneous[a]	Y[a]	3.43 ± 0.96	208.74 ± 0.96	297.10 ± 2.12
Montdenier	Rochette	190	Igneous	N	9.42 ± 0.96	219.27 ± 0.96	192.99 ± 2.12
Montagnac	Rochette	196	Igneous	N	17.70 ± 0.96	225.96 ± 0.96	196.86 ± 2.12
Salette	Brac	262	Igneous	Y	17.78 ± 0.96	81.51 ± 0.96	254.59 ± 2.12
Coulettes	Brac	271	Igneous	Y	14.50 ± 0.96	78.68 ± 0.96	222.51 ± 2.12
Robine	Issole	295	Igneous	Y	5.36 ± 0.96	225.58 ± 0.96	236.45 ± 2.12
Malay	Issole	337	Igneous	Y	2.72 ± 0.96	77.64 ± 0.96	283.05 ± 2.12
Hahonih	Sid	371	Igneous	Y	21.41 ± 0.96	73.18 ± 0.96	127.00 ± 2.12
Atsah	Sid	374	Igneous	Y	18.02 ± 0.96	69.87 ± 0.96	111.91 ± 2.12
Swift Run	Skinner Ridge	490	Sedimentary	Y	16.63 ± 0.96	355.94 ± 0.96	220.71 ± 2.12
Skyland	Skinner Ridge	495	Sedimentary	Y	17.18 ± 0.96	4.68 ± 0.96	240.38 ± 2.12
Hazeltop	Wildcat Ridge	509	Sedimentary	Y	13.78 ± 0.96	3.53 ± 0.96	341.30 ± 2.12
Bearwallow	Wildcat Ridge	516	Sedimentary	Y	15.28 ± 0.96	358.37 ± 0.96	333.17 ± 2.12[b]
Shuyak	Amalik	575	Sedimentary	Y	16.72 ± 0.96	219.48 ± 0.96	259.41 ± 2.12
Mageik	Amalik	579	Sedimentary	Y	26.11 ± 0.96	198.38 ± 0.96	91.18 ± 2.12
Kukaklek	Hidden Harbor	623	Sedimentary	Y	6.15 ± 0.96	289.36 ± 0.96	265.10 ± 2.12
Atmo Mountain	Observation Mountain	634	Regolith	N	–	–	–
Crosswind Lake	Observation Mountain	639	Regolith	N	–	–	–
Melyn	Tenby	749	Sedimentary	Y	6.49 ± 0.96	258.59 ± 0.96	222.44 ± 2.12[b]
Otis Peak	Emerald Lake	822	Sedimentary	Y	4.63 ± 1.00	182.83 ± 1.00	180.13 ± 2.14
Pilot Mountain	Hague Creek	882	Sedimentary	Y	2.00 ± 0.96	262.69 ± 0.96	234.21 ± 2.12
Pelican Point	Hans Amundsen Memorial Workspace	923	Sedimentary	Y	1.29 ± 0.96	246.80 ± 0.96	218.91 ± 2.12[b]
Lefroy Bay	Lake Newell	942	Sedimentary	Y	0.53 ± 0.96	55.66 ± 0.96	122.08 ± 2.12[b]

Note. The first column lists the sample name, the second column lists the sampling location, the third column lists the sampling sol, the fourth column lists the sample lithology, the fifth column lists whether the sample was acquired from in situ bedrock, and the sixth through eighth columns list the hade, azimuth and roll and upper limits on their 3σ uncertainties. The reported hades and azimuths are taken from the post-coring pre-unloading Front Hazcam Left images. The uncertainties are estimated as discussed in Section 2.6 with a breakdown shown in Table 3. [a]Due to crumbling of the rock during drilling, the sample tube contains the Martian atmosphere and possibly a few unoriented grains of rock. [b]Core top marked with SuperCam laser for roll orientation.

composition) and the remaining 12 from sedimentary rocks (siltstones and sandstones with either bulk basaltic or sulfate-rich compositions) (Table 1). The remaining 2 cores (Montdenier and Montagnac) were acquired from a ∼40-cm diameter tabular igneous boulder that was differentially tilted with respect to adjacent bedrock and moved during the course of drilling. Future laboratory measurements on this unique sample suite should collectively enable many of the aforementioned studies of the igneous, sedimentological, tectonic and magnetic evolution of Mars (Section 1.1).

2. Core Orientation Methodology

2.1. Orienting the Core by Orienting the Coring Drill

Mars 2020 samples are acquired with the Coring Drill (referred to hereafter as the Drill), a rotary percussive drilling mechanism at the end of the rover arm (Moeller et al., 2021) (Figure 2). The Drill employs a Coring Bit (a 27-mm outer diameter, 185-mm long stainless steel cylinder coated with titanium nitride and tipped with 4 tungsten carbide teeth) containing an interior Sample Tube. Core samples are typically 13 mm in diameter and 61–81 mm long, such that the typical kerf is 7 mm. The Drill can acquire cores at an angle of up to 10° between the Drill axis (pointing vector) and surface normal and at an angle up to 110° from local gravity (i.e., 20° up from geographic horizontal).

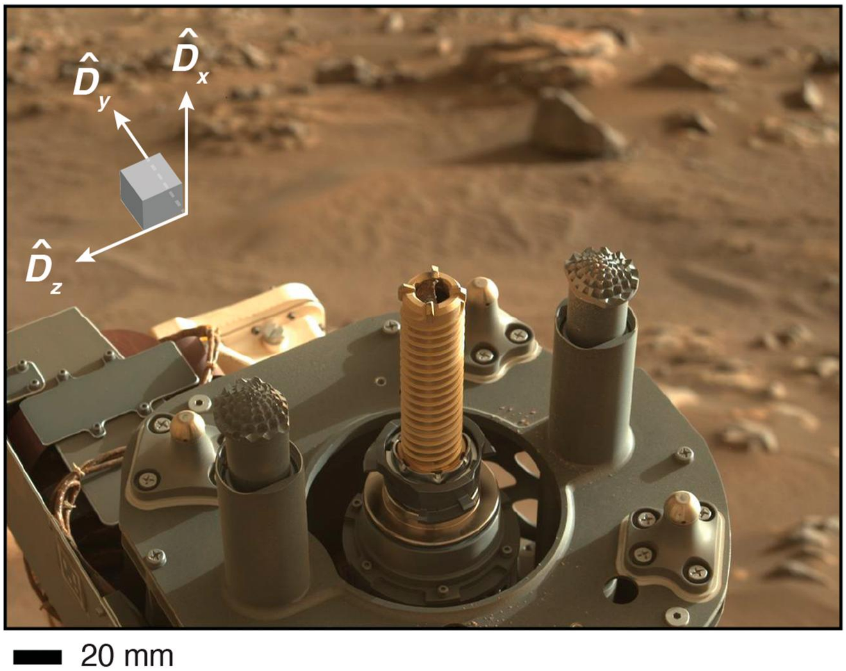

& J - #/ - AN - 2
? - 9 4 - ?
? - - - - -
- - 7 A(7 ?
- 4 ? 4 4
N 8R8#/ R8, 3311/ 8/ R/' ' 2 KR&8 8 81N 8*8/ 8R8#' 8 8

*S#8 U , S/
? % @& 2 8 ? 9 -
* ' # ? 3 ' # ? . - -
2) ? . #?

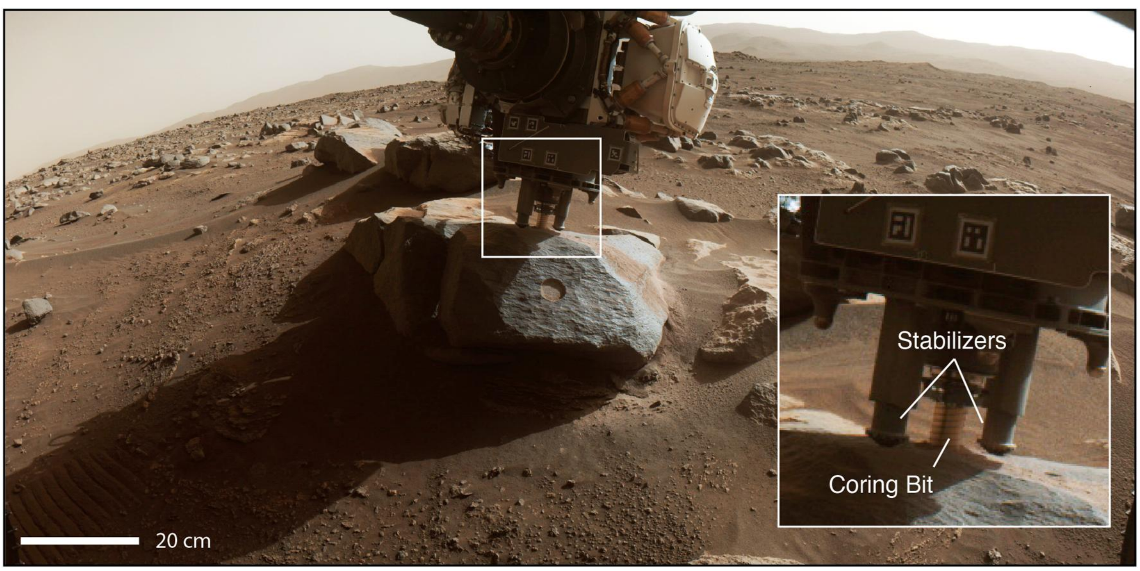

& . 6) : 9 - #/ ' ?
4
. . R8#/ ' R8/ 88 * 81/ R*8, % R&8 8 81. 6 N883 R8 8 3* 8

Table 2
Reference Frames Relevant for Orienting Perseverance Cores on Mars

Name	Notation	x	y	z
Rover Mechanical	$\hat{R}_x - \hat{R}_y - \hat{R}_z$	Rover forward	Starboard	Rover down
Drill	$\hat{D}_x - \hat{D}_y - \hat{D}_z$	Drill axis away from rover	Perpendicular to axis containing Stabilizers toward PIXL	Along axis containing Stabilizers
WATSON	$\hat{W}_x - \hat{W}_y - \hat{W}_z$	Normal to WATSON image plane toward outcrop	In WATSON image plane toward top of image[a]	In WATSON image plane toward right of image[a]
Geographic	$\hat{G}_x - \hat{G}_y - \hat{G}_z$	North	East[b]	Down[b]
Site frame i	$\hat{S}_{x,i} - \hat{S}_{y,i} - \hat{S}_{z,i}$	Estimated north	Estimated east[c]	Estimated down[c]
Core	$\hat{C}_x - \hat{C}_y - \hat{C}_z$	Core axis into outcrop (core pointing vector)	Upward along steepest direction of plane normal to $\hat{C}_x$	In Martian horizontal plane

Note. The first column lists the coordinate system name and the next three columns define the orientations of the x-, y-, and z-axes. All coordinate systems are right-handed: $\hat{A}_x \times \hat{A}_y = \hat{A}_z$. [a]The $\hat{W}_y - \hat{W}_z$ plane is called the "WATSON plane." [b]The $\hat{C}_y - \hat{C}_z$ plane is called the "Core plane." [c]The $\hat{S}_x - \hat{S}_y$ plane is called the "Site horizontal plane."

between the Martian Geographic and various Site frames in the rest of this manuscript and we will drop the Site frame subscript, i. We will use the terms "Site horizontal" to denote the $\hat{S}_x$-$\hat{S}_y$ planes and "Site down" and "Site up" to denote the axial directions parallel and antiparallel, respectively, to $\hat{S}_z$ (Figure 6).

Finally, we define the core frame as having $\hat{C}_x$ pointing along the core into the outcrop, $\hat{C}_y$ pointing upward along the steepest direction of the plane normal to $\hat{C}_x$ (i.e., $\hat{C}_x - \hat{C}_y$ lies in the Site vertical plane), and $\hat{C}_z$ lying in the Martian geographic horizontal plane, completing the triad (Figure 6). We refer to the $\hat{C}_y - \hat{C}_z$ plane as the "Core plane," which may be canted with respect to the outcrop surface and with respect to the WATSON plan. $\hat{C}_x$ is to

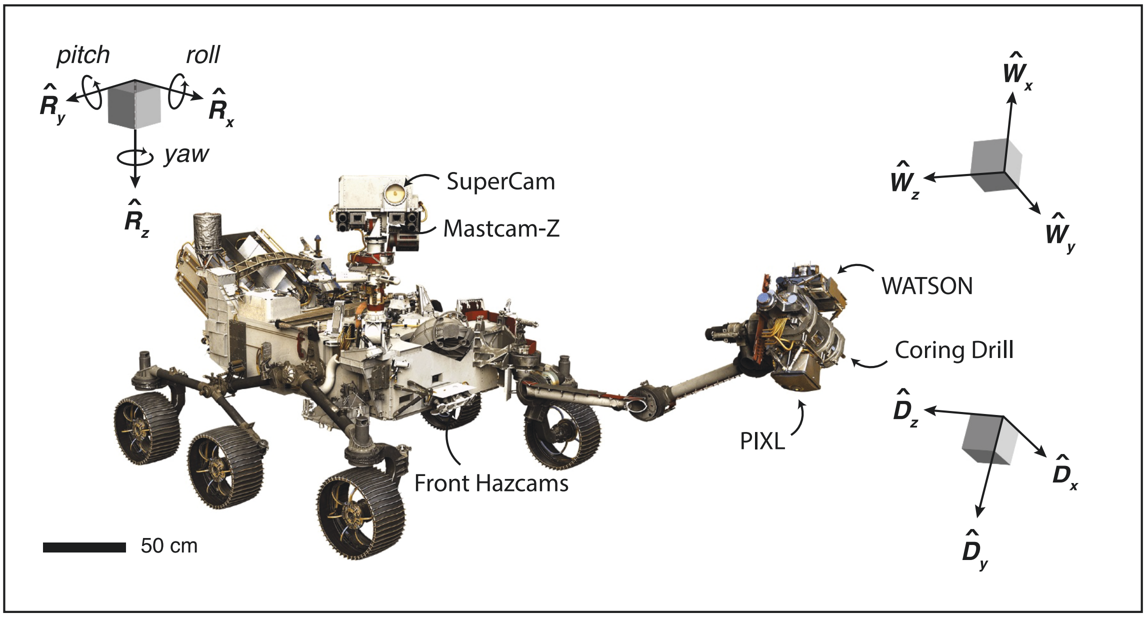

Figure 4. Rover Mechanical, Wide Angle Topographic Sensor for Operations and eNgineering (WATSON), and Drill coordinate systems for Perseverance rover. Shown is a drawing of the rover with orientations of the three coordinate systems. For the Rover Mechanical system (R_x, R_y, R_z), $\hat{R}_x$ points forward, $\hat{R}_y$ points to starboard, and $\hat{R}_z$ points down. For the WATSON system (W_x, W_y, W_z), $\hat{W}_x$ points perpendicularly out of the image plane, $\hat{W}_y$ points to the top of the image plane and $\hat{W}_z$, points toward the right of the image plane (see Figures 6–8 and 11–13). For the Drill frame (D_x, D_y, D_z), $\hat{D}_x$ points along the drill shaft, $\hat{D}_y$ points perpendicular to the axis containing the two Stabilizers toward the Planetary Instrument for X-Ray Lithochemistry (PIXL) instrument, and $\hat{D}_z$ axis points along the axis of the Stabilizers. PIXL, the Coring Drill, Front Hazcams, SuperCam and Mastcam-Z are labeled.

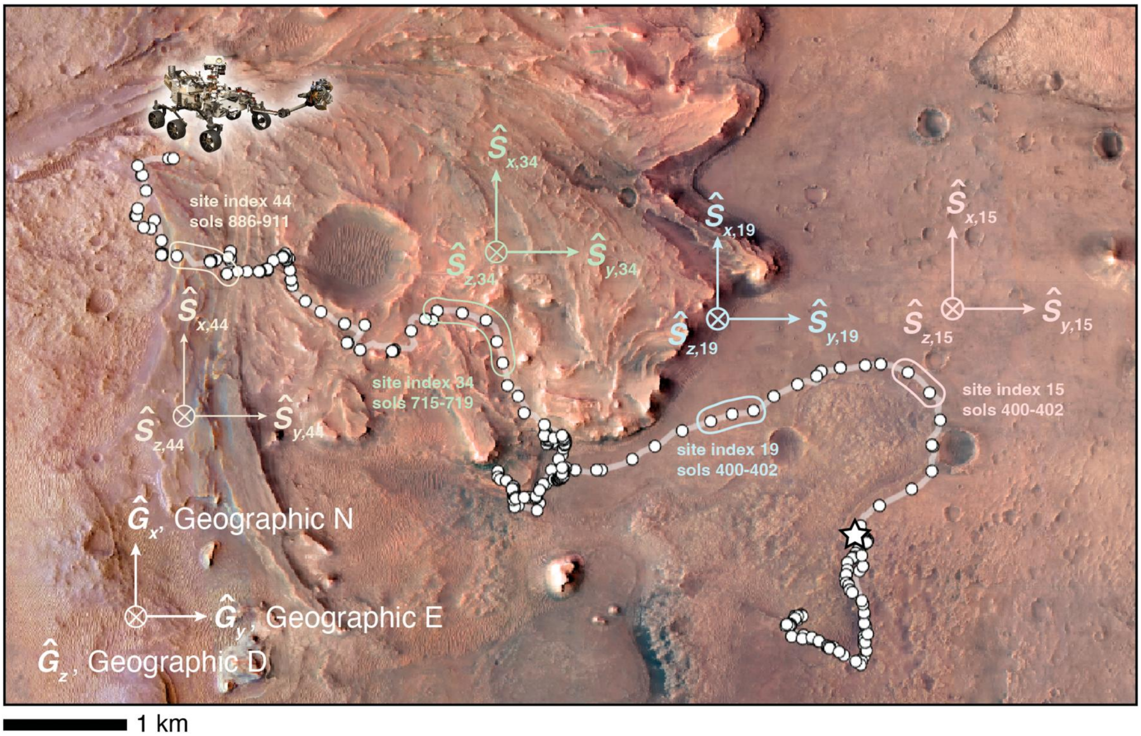

& 5 6 (4 6 (? -
3, 8 % - - -
A ? 3, 8 @ 2 -
- - - ' - &? ' - ? '
- ? 4 4 *) ? 4 3 ? 4 #' ? 4 ' ' ?
4 - B : 4 5

8 B? - ? -

. &

A - 4 A
4
4 88, ? 2 -
; .
; - : 2 G
33 ? - 4 : . , ? &

- -
,

% :
4 & 38B -
) - - ? 9
9

, 9 9

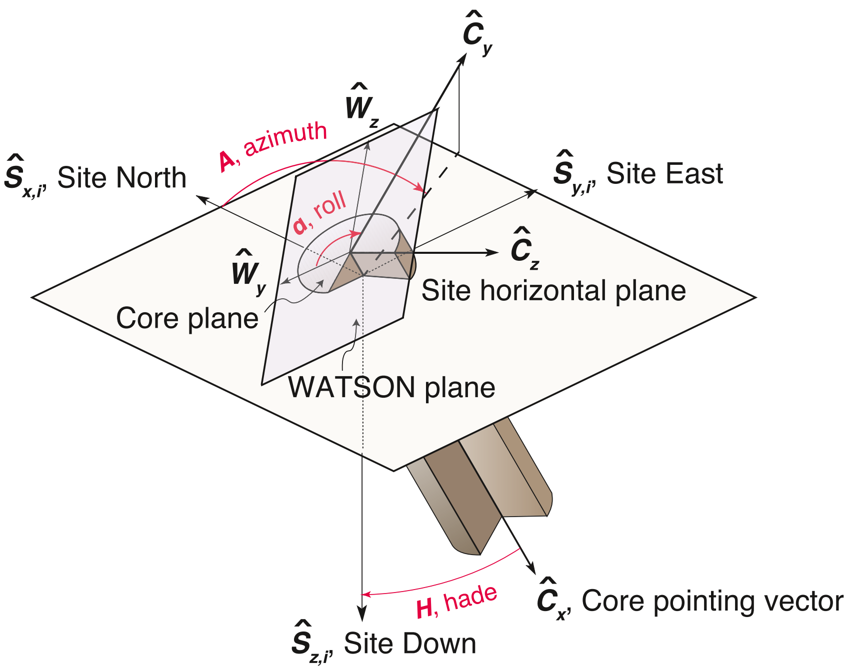

& 3 - - -
- : - 4 4
? -
?
) - 9
?) -
% @ & % @&? A A4 &
9 A4 % @& 9& & 4 % @&
9& & 2 33 ?

) - % @& &
9 % @& 9& &
& , 9& & 9& & #

, &

: S# : & 4
: % @& 8 8
: -
A 4 4 :
5 8 ?

-

- -

-

-

Q - . 4
-

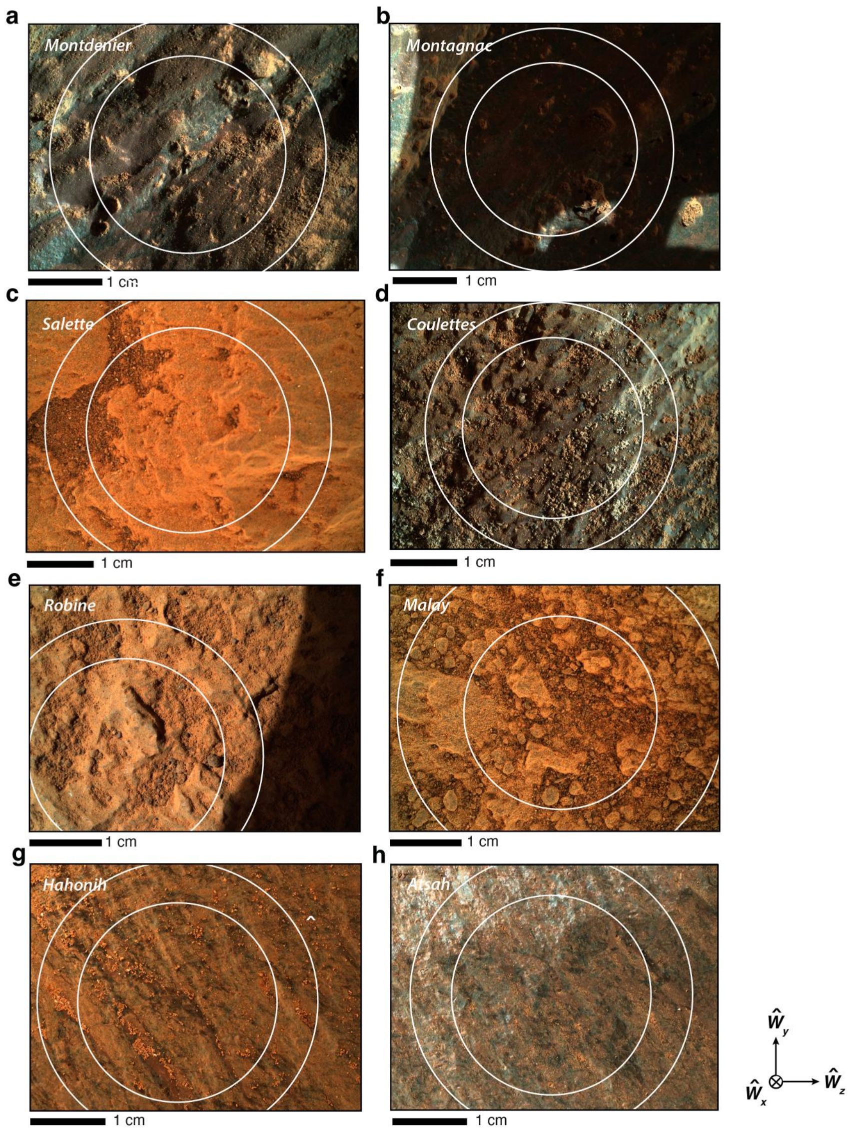

& 4 % @ & % @&?
- ? 11? % @&
. R8 11R8, 1#, ' ##, ' R#* . (R&88/ 8888 (88, / 1R8888 8 ? 3*? % @&
. R8 3*R8, 1' ***/ / R#38. (R&88/ 8888 (88/ 8 R8888 8 ? */ ? % @&
. R8 */ R8, 13/ *, 18 R81*. (R&8818888 (88, *' R8888 8 ? , / ? % @&
. R8 , / R8, 38, , / R11, . (R&8818888 (88/ 8 R8888 8 ? (3#? % @&
. R8 3#R8, 3 3*/ , 1#R#31. (R&8838888 (88, ' #R8888 8 ? ##/ ? % @&
. R8##/ R8, 3, 1*3 R , / . (R&8838 / , (88, #, R8888 8 ?6 #/ 8? % @&
. R8#/ 8R8, 33/ 3* 11R13' (R&8 8 81 (88, , #R8888 8 ? #/ #? % @&
. R8#/ #R8/ 888, **8*R' 8 (R&8 8 81 (88, */ R8888 8 - % @&
& & & ? - / A
2 @ - 2 - #
H * ' ?S ? ?S ? 3 '
? #/ 1 ' * 1 &)
) ?

& % @& I8 8M % @&
(:
: % @& (& ?
(& ? % @&

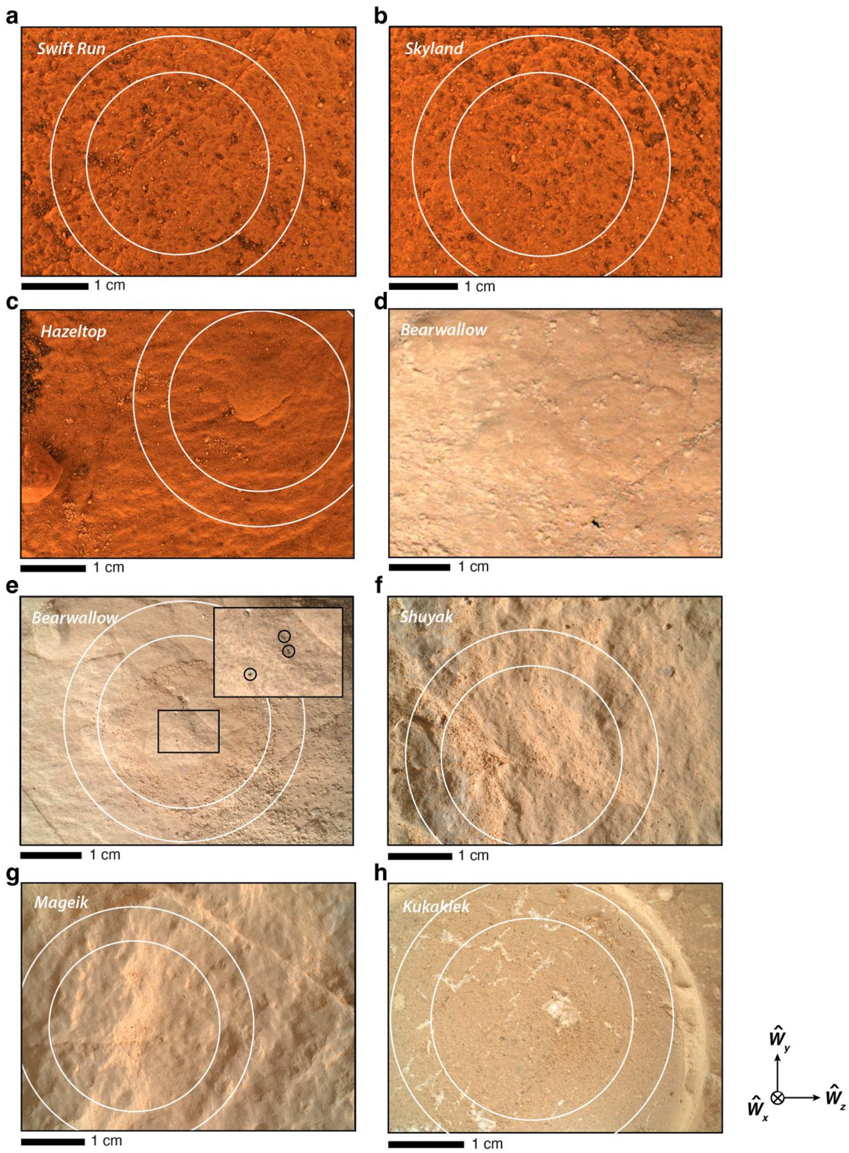

& 5 % @ & % @&?
- ? - (' 1*? % @&
. R8' 1*R8/ 8333' / **R . (R&8 , 88' (88/ #8R8888 8 ?) ' 1*? % @&
. R8' 1*R8/ 8333, 8 ' R1, / . (R&8 , 88' (88/ #8R8888 8 ?6 *8*? % @&
. R8*8*R8/ / / # , R8 *(R&8 , (88/ #8R8888 8 ? 2 - -
8? % @& . R8*8*R8/ / / ' 1# R# 1. (R&8 , (8' 88 R8888 8 ? 2 - -
) - A * ? 2 4 -
% @& . R8* R8/ # ' 3**R/ , . (R&8 , (88/ / #R8888 8
?) */ 8? % @& . R8*/ 8R8/ / ** / 1' R/ , *. (R&8 38888 (88/ *8R8888 8
?) */ / ? % @& . R8*/ / R8/ 1 / 8/ *' R*, . (R&8 38888 (88/ 8 R8888 8
? 0))) , ' ? % @&
. R8, ' R8/ ' **' ' R/ #' . (R&8#8 / (88, ' #R8888 8 - % @&
& & & ? - / A
2 @ - 2 - #
. * ' - ?S ? ?S ? &
)) ?
4 2 - - ?

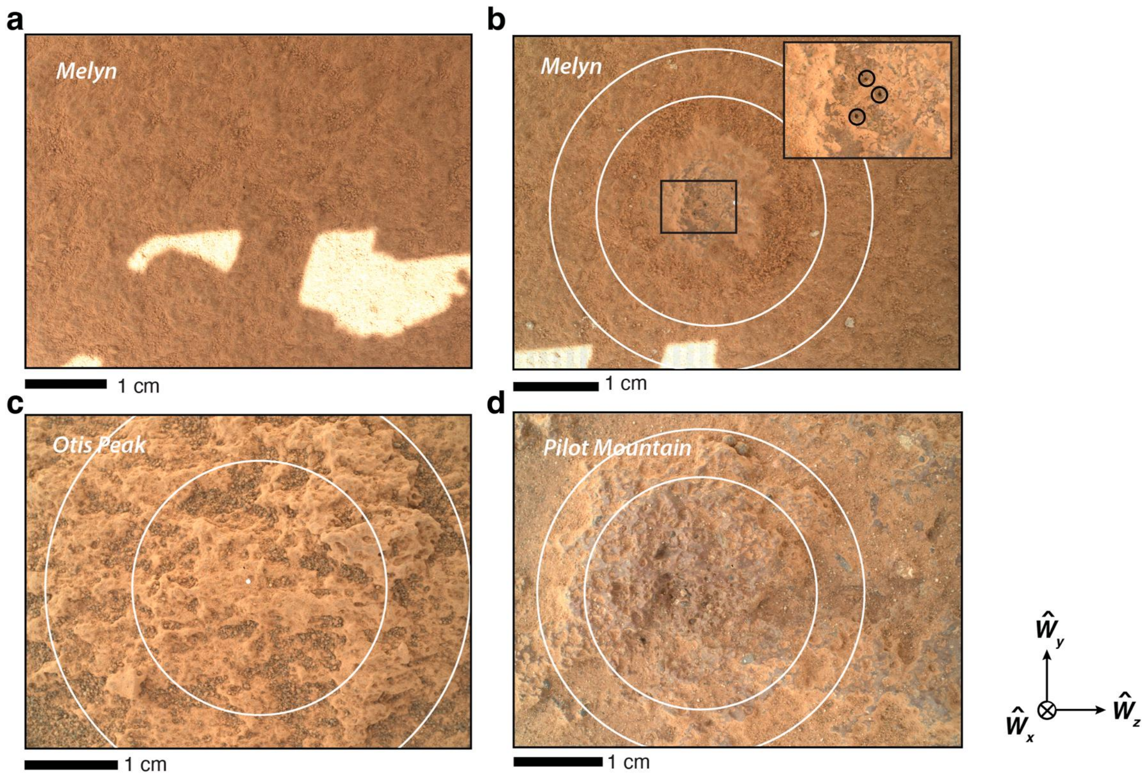

& 7 % @ & % @&? -
? /' ?) % @&
. R8/' R8/# / 1, 3 R' 18(R&8#/ 8888 (88/ 8 R8888 8 ?) - A
/'/? 2 4 - % @& . R8/' / R8/ ## *3, , 1R 1. (R&8#/ 8888 (88/' 1R8888 8
? @) 1 ? % @& . R81 R8/ #33 # 8 R*88. (R&8' 88 # (88, , 8R8888 8 ? 1/ 3?
% @& . R81/ 3R8/' ' 3/ / 38*R*' , . (R&8' #8888 (88/' #R8888 8 ?S ? -
2 / ? @ - 2 - #
*' ? ? 3' ? #/ 1 ' * 1

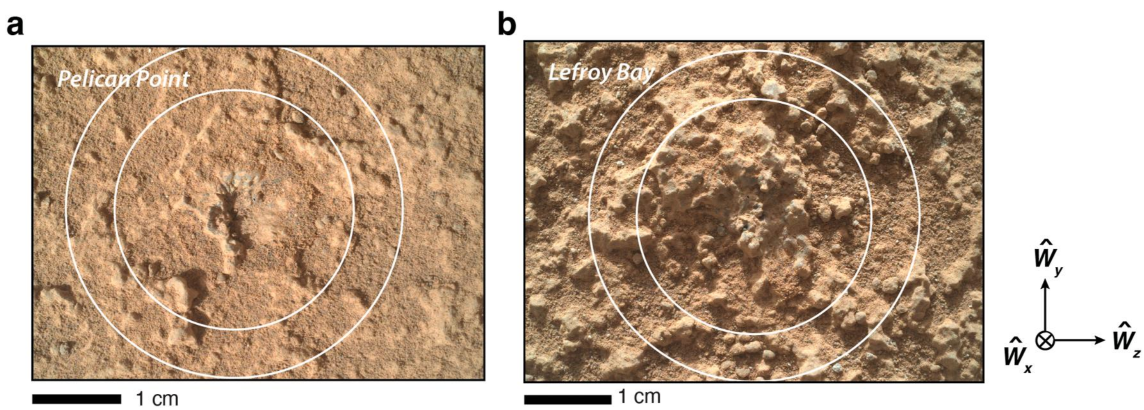

& 9 % @ & % @&? -
? 3 8? % @& . R83 8R8/' 1, # / R, # . (R&8' *8888 (88/ #/ R8888 8 ? 2 3#1?
% @& . R83#1R8/ *8 , 81/ R888. (R&8' , 8888 (88/' 1R8888 8 -
2 / ? @ - 2 - #
. *'


a
Uniform Saddleback Basalt
b
Napa Basaltic Sandstone
c
Bishop Tuff Intermediate
d
China Ranch Gypsum
e
Kramer Massive Mudstone
10 mm
D_x, Drill pointing vector

10.1029/2023EA003322

Table 3
Uncertainty Estimates for the First 21 Rock Coring Attempts by the Perseverance Rover

Uncertainty term	All but Otis Peak (°)	Otis Peak (°)
ϵ_{bll}	0.881	0.881
ϵ_{SU}	0	<0.141[a]
ΔH_{bll}	0.509	<0.590[b]
ΔH_{Db}	<0.810	<0.810
ΔH_o	<0.031	<0.031
$\boldsymbol{\Delta H}$	**0.957**	**1.003**
ΔA_{bll}	0.509	<0.590[b]
ΔA_{Db}	<0.810	<0.810
ΔA_o	<0.680	<0.680
$\boldsymbol{\Delta A}$	**1.174**	**1.211**
$\Delta \alpha_{bll}$	0.509	<0.590[b]
$\Delta \alpha_{Wb}$	<2.060	<2.060
$\boldsymbol{\Delta \alpha}$	**<2.122**	**<2.143**
Total	**<2.607**	**<2.658**

Note. The first column lists term in the uncertainty budget, value for all cores except Otis Peak (3σ), and the third column lists the value for Otis Peak (3σ). The uncertainties are estimated as discussed in Section 2.6. [a]Estimated using a delay since last sunID update of $\Delta t = 10$ min. [b]Assumes that the uncertainty in rover orientation following the last sunID update is evenly apportioned between the hade, ΔH_{bll}, azimuth, ΔA_{bll}, and roll, $\Delta \alpha_{bll}$ In fact, the sunID update mainly improves the yaw uncertainty, which in general is not equally apportioned to the uncertainty in hade, azimuth, and roll. We ignore this complication because of the very small magnitudes of ϵ_{SU}.

$$\hat{D}_{y,\mathrm{Site}}(t_W) = \frac{\left[\hat{D}_{x,\mathrm{Site}}(t_W) \times \hat{S}_{z,\mathrm{Site}}(t_W)\right] \times \hat{D}_{x,\mathrm{Site}}(t_W)}{\left|\left[\hat{D}_{x,\mathrm{Site}}(t_W) \times \hat{S}_{z,\mathrm{Site}}(t_W)\right] \times \hat{D}_{x,\mathrm{Site}}(t_W)\right|}$$

We then project this onto the WATSON plane:

$$\mathrm{proj}_{\hat{W}_y - \hat{W}_z}\left[\hat{D}_{y,\mathrm{Site}}(t_W)\right] = \mathrm{proj}_{\hat{W}_x}\left[\hat{D}_{y,\mathrm{Site}}(t_W)\right] - \hat{D}_{y,\mathrm{Site}}(t_W) \tag{9}$$

where $\mathrm{proj}_{\hat{W}_x}(\hat{D}_y) = \left[\hat{D}_y \cdot \hat{W}_x\right]\hat{W}_x$ is the projection of $\hat{D}_y$ on $\hat{W}_x$. With $\hat{C}_{y,\mathrm{Site}}(t_W) \approx \hat{D}_{y,\mathrm{Site}}(t_W)$, the roll can now be estimated by substituting Equations 8 and 9 into Equation 3.

Translation of the direction $\hat{C}_y$ in the WATSON image to the core after it is returned to Earth requires identification of azimuthally asymmetric features on the core top. These rotationally asymmetrical features on the natural core top including nodules or bumps, crevices, and other markings that will be easily recognizable.

For cores lacking such natural markings, rotationally asymmetric artificial markings can be made on the core top using the laser on the SuperCam instrument (Maurice et al., 2021; Wiens et al., 2021). In particular, we have developed a procedure in which three distinct pits are produced on the outcrop surface prior to drilling in the shape of an "L" (∼2.5 mm × ∼1 mm) using 125 laser pulses lasting 4 ns each. The number of pits and their arrangement were chosen to meet four competing priorities. The first priority, addressed by maximizing the number of pits, is that the core surface must be successfully marked despite the typical lateral uncertainty in placement of the Drill. The second priority, addressed by maximizing the depth of each pit, is that the outside surface of the core must retain the marks until it is returned to Earth given the possibility that it could be damaged during or after drilling. The third and fourth priorities, addressed by minimizing both the number of pits and their depths, were to minimize laser damage to the core surface area and core volume and to reduce rover operational complexity and power consumption.

2.5.3. Propagating Orientation Into Core Body

The above description of the core orientation procedure assumes the core is returned to Earth as a solid object that is not internally differentially rotated during or after drilling. Because the only constraint on the state of internal deformation following drilling are from CacheCam images of the core bottom, the overall mechanical states of the drilled cores will be essentially unknown until they are returned to Earth. In fact, coring of a diversity of rock lithologies using the Mars 2020 Qualification Model Dirty Testing (QMDT) testbed at the Jet Propulsion Laboratory (JPL) found that essentially all cores fractured during drilling (see Figure 48 of Moeller et al. (2021)). Well-indurated lithologies with weak foliation (e.g., basalts, basaltic sandstones, and rhyolitic tuffs) typically produced fragments with well-preserved fracture planes (Figure 11). However, softer and more foliated lithologies (e.g., mudstones, hydrated sulfates) commonly produced fragments in the form of wafers or occasionally even pulverized pebbles and granules (Figure 11).

For fragmented cores, the full core orientation (hade, azimuth, and roll) can be propagated into the core from the outer surface imaged by WATSON by rotating the fragments so that they fit together and lock into place like puzzle pieces. Computerized tomography scanning of the core in the sample receiving laboratory prior to extraction (e.g., Ziegler et al., 2021) would be very valuable for documenting the orientation relationships of fragments. The first depth at which pieces cannot be reassembled in this way to their original orientations sets the maximum depth to which the full orientation can be propagated using surface images. This maximum depth is highly dependent on core lithology; images of QMDT test cores show that it ranges from ∼20% to 100% of the core length for the indurated lithologies and ∼0%–40% for the soft and foliated lithologies (Figure 10). It is

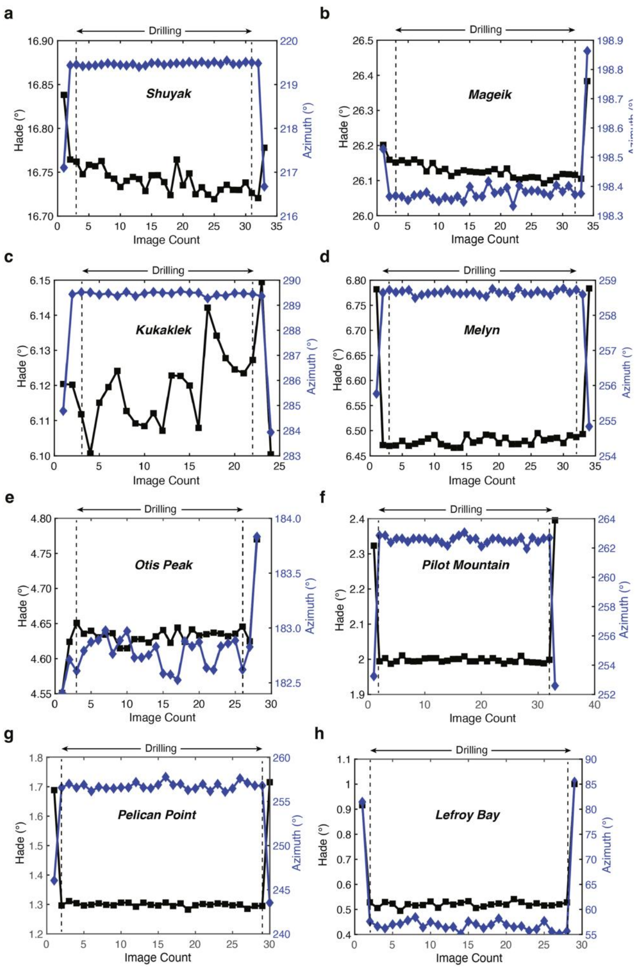
a
Drilling
Shuyak
Hade (°)
Azimuth (°)
Image Count
b
Drilling
Mageik
Hade (°)
Image Count
c
Drilling
Kukaklek
Hade (°)
Azimuth (°)
Image Count
d
Drilling
Melyn
Hade (°)
Azimuth (°)
Image Count
e
Drilling
Otis Peak
Hade (°)
Azimuth (°)
Image Count
f
Drilling
Pilot Mountain
Hade (°)
Azimuth (°)
Image Count
g
Drilling
Pelican Point
Hade (°)
Azimuth (°)
Image Count
h
Drilling
Lefroy Bay
Hade (°)
Azimuth (°)
Image Count

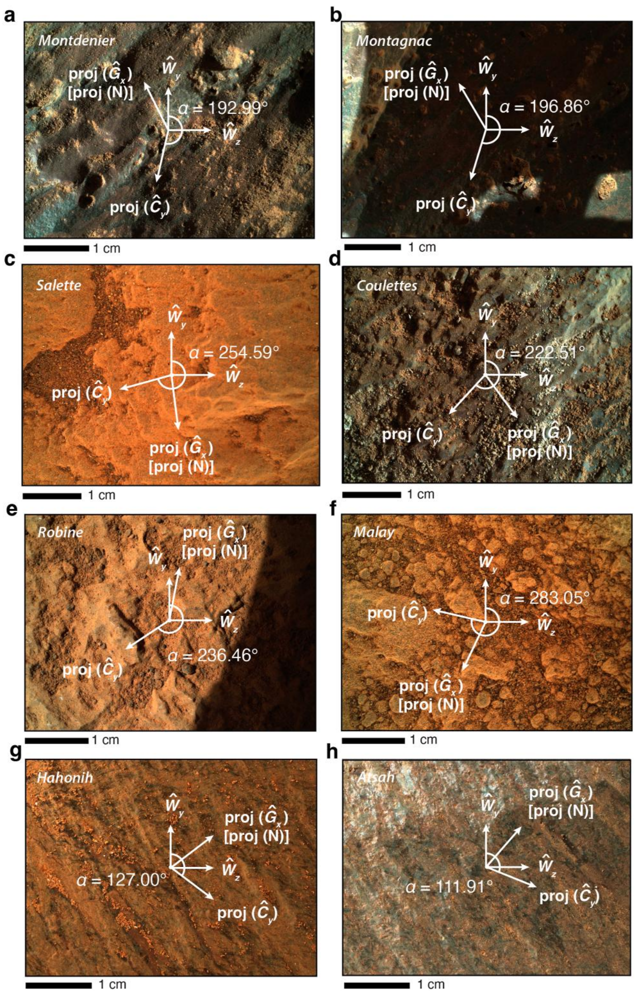
a
Montdenier
proj ($\hat{G}_x$)
[proj (N)]
$\hat{W}_y$
α = 192.99°
$\hat{W}_z$
proj ($\hat{C}_y$)
1 cm
b
Montagnac
proj ($\hat{G}_x$)
[proj (N)]
$\hat{W}_y$
α = 196.86°
$\hat{W}_z$
proj ($\hat{C}_y$)
1 cm
c
Salette
$\hat{W}_y$
α = 254.59°
$\hat{W}_z$
proj ($\hat{C}_y$)
proj ($\hat{G}_x$)
[proj (N)]
1 cm
d
Coulettes
$\hat{W}_y$
α = 222.51°
$\hat{W}_z$
proj ($\hat{C}_y$)
proj ($\hat{G}_x$)
[proj (N)]
1 cm
e
Robine
proj ($\hat{G}_x$)
[proj (N)]
$\hat{W}_y$
$\hat{W}_z$
α = 236.46°
proj ($\hat{C}_y$)
1 cm
f
Malay
$\hat{W}_y$
proj ($\hat{C}_y$)
α = 283.05°
$\hat{W}_z$
proj ($\hat{G}_x$)
[proj (N)]
1 cm
g
Hahonih
$\hat{W}_y$
proj ($\hat{G}_x$)
[proj (N)]
$\hat{W}_z$
α = 127.00°
proj ($\hat{C}_y$)
1 cm
h
Atsah
proj ($\hat{G}_x$)
[proj (N)]
$\hat{W}_y$
$\hat{W}_z$
α = 111.91°
proj ($\hat{C}_y$)
1 cm

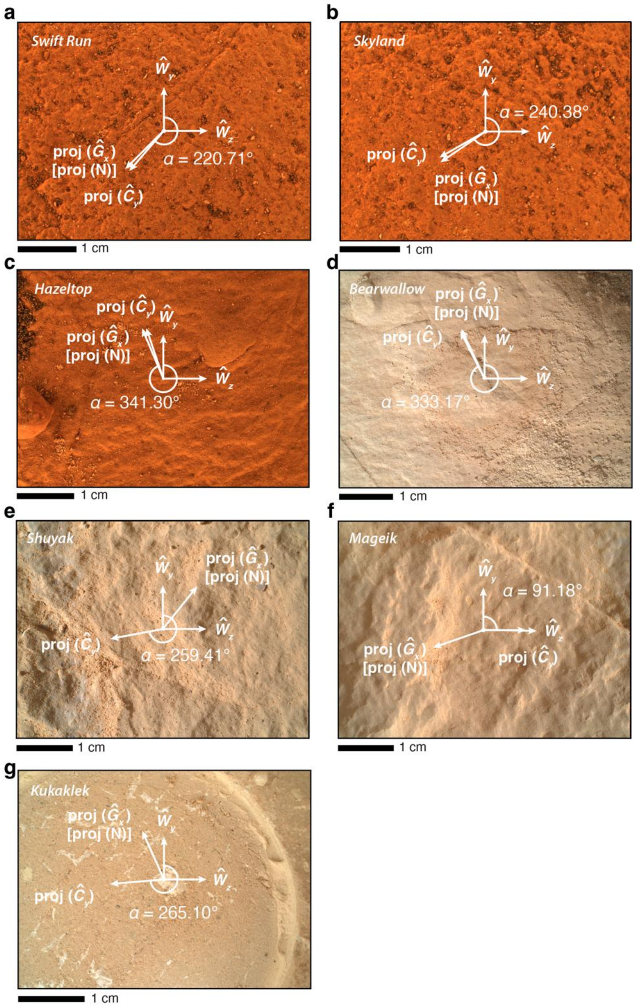

& , % @ &
% @&? -)
% @& A
A4 & & ?) - &
9 A4 % @&
- 9 5 9 ' ?
% @& ? - (% @& . R8' 1*R8/ 83
33' / **R . (R&8 , 88' (88/ #8R8888 8 ?)
% @& . R8' 1*R8/ 8333, 8 ' R1, / . (R&8 , 88' (88/ #8R8
888 8 ? 6 % @& . R8*8*R8/ / / # , R8
*(R&8 , (88/ #8R8888 8 ? 2 - - % @&
. R8* R8/ # ' 3**R/ , . (R&8 , (88/ / #R8888 8
?) % @& . R8*/ 8R8/ / ** / 1' R/ , *. (R&8
38888 (88/ *8R8888 8 ?) % @&
. R8*/ / R8/ 1 / 8/ *' R*, . (R&8 38888 (88/ 8 R8888 8
? 0))) % @& . R8, ' R8/ ' **' ' R/ #' . (R
&8#8 / (88, ' #R8888 8

- :

/

- / , B @) / B @)
#?

0

& 0 &

% 8) -
(2
:
: 8 ? -

%
, ? .) -
9
9 9
-
- 8 B 8 8 1B . 1
) - -
- 8S#8 - -
: . 6 . ' ? . G
- # 8 8# B
8 , 1B 1 . H S 1?
2 A
- #

8)) -
- % @&
)
-
-
. #? . ' ? . *?
. , ? %
)
. / 1 S1 1 S1 3 ? 6 - -
[2 - - [ )
) -)
. 1 1 3 3 ?
) -
4

) - 4
) -
6 - - 4
% @&
- ' ' B - / 31B 4

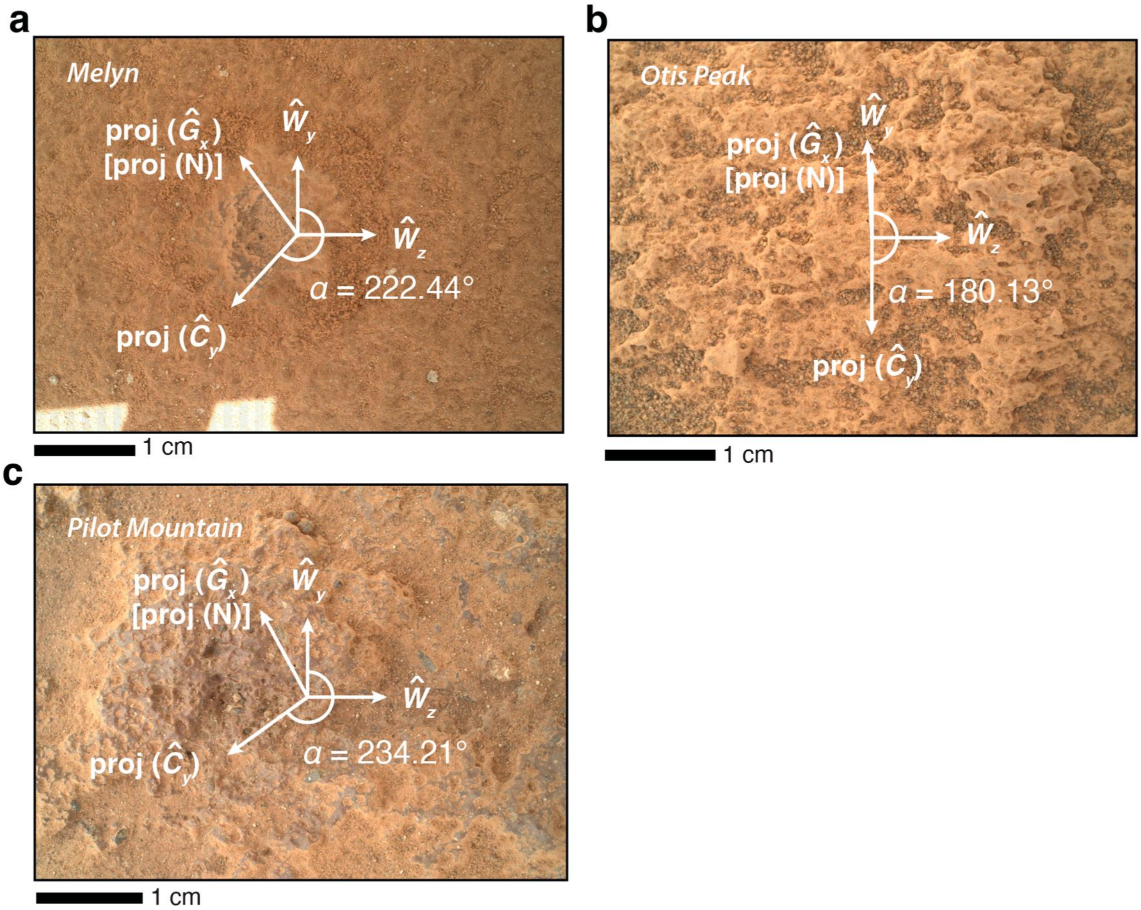

& % @ & % @&? -)
% @& A A4 & & ?) - & 9 A
4 % @& - 9 5 9 ' ? % @& ? % @&
. R8/ ' / R8/ ## *3, , 1R 1. (R&8#/ 8888 (88/ ' 1R8888 8 ? @) % @& . R81 R8/ #33 # 8 R*88. (R&8' 88 # (
88, , 8R8888 8 ? % @& . R81/ 3R8/ ' ' 3/ / 38*R*' , . (R&8' #8888 (88/ ' #R8888 8

((-) - -
' / 3#B

, 6

(.
8 ?
7 A
.
% @&

&

8 8 9 : :
) . - -)
-) / B # ?
@ 8) 1 - :)
4

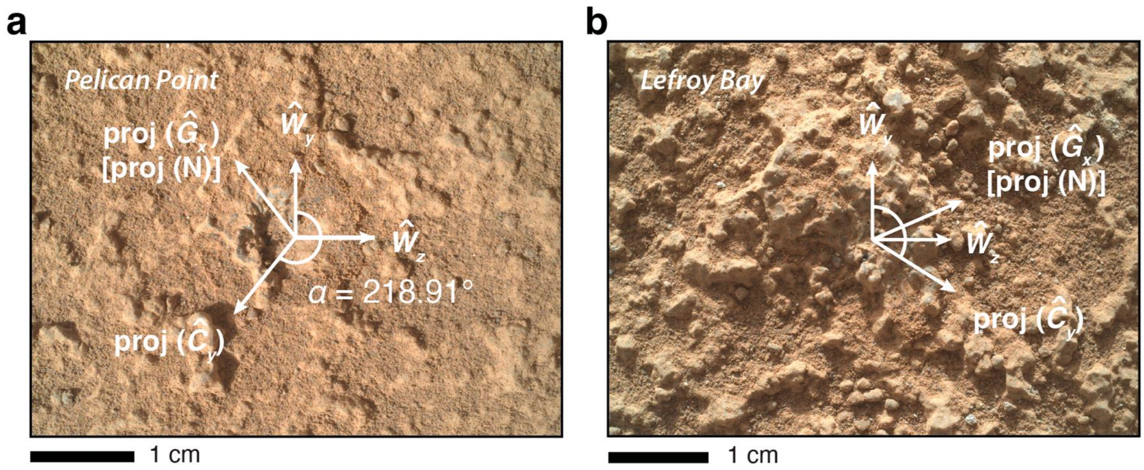
a
Pelican Point
proj (Ĝx)
[proj (N)]
Ŵy
Ŵz
α = 218.91°
proj (Ĉy)
1 cm
b
Lefroy Bay
Ŵy
proj (Ĝx)
[proj (N)]
Ŵz
proj (Ĉy)
1 cm